ZO-1 regulates stress granule formation in endothelial cells by interacting with YB-1

Yassine El Bakkouri
Université de Montréal
Rony Chidiac
University of Toronto https://orcid.org/0000-0002-3642-0651
Jeanne Corriveau
Université de Montréal
Vanda Gaonac'h-Lovejoy
Université de Montréal
Ashley Chin
Institut de recherches cliniques de Montréal (IRCM)
Éric Lécuyer
Institut de recherches cliniques de Montréal (IRCM)
Stephane Angers
University of Toronto https://orcid.org/0000-0001-7241-9044
Ivan Topisirovic
Lady Davis Institute https://orcid.org/0000-0002-5510-9762
Laura Hulea
University of Montreal
Chantal Delisle
Université de Montréal
Jean-Philippe Gratton (jean-philippe.gratton@umontreal.ca)
Université de Montréal https://orcid.org/0000-0001-9877-8520

Article

Keywords: ZO-1, stress granules, YB-1, endothelial cells, angiogenesis, retina

Posted Date: January 17th, 2022

DOI: https://doi.org/10.21203/rs.3.rs-1200419/v1

Abstract

Zonal occludens-1 (ZO-1) is involved in the regulation of cell-cell junctions between endothelial cells (ECs). Here, we define the ZO-1 protein interactome and reveal novel ZO-1 interactions with RNA binding proteins (RBP) that are part of stress granules (SGs). Exposure of ECs to stresses decreased ZO-1 protein levels which was accompanied by increased SG formation and protection of ECs from cellular insults. We uncovered a previously undocumented association between ZO-1 and Y-box Binding Protein 1 (YB-1). Arsenite treatment of ECs decreased the interaction between ZO-1 and YB-1. In turn, downregulation of ZO-1 increased the association of YB-1 and G3BP1, thus driving SG assembly. Importantly, YB-1 is essential for the protective effects induced by downregulation of ZO-1 and SG formation. Finally, in the developing retinal vascular plexus of newborn mice, ECs at the extremities of growing vessels express less ZO-1 and display more YB-1 positive SGs than ECs located in the median portion of the retinal vasculature. Together, our findings demonstrate an unsuspected role for ZO-1 in SG formation, through its interaction with YB-1, and in the response of ECs to stresses during angiogenesis.

Introduction

Cell-cell junctions between endothelial cells (ECs) are constantly remodelled during the formation of new blood vessels [1, 2]. Intercellular junctions between ECs are generally formed by homotypic interactions between transmembrane proteins connected to a network of intracellular cytosolic proteins that integrate signaling events essential for angiogenesis [3]. Genetic deletion of the cell junction proteins VE-cadherin, β-catenin or Zonal occludens-1 (ZO-1) in ECs of mice leads to embryonic lethally due to vascular defects [4–7]. The tight junction protein ZO-1 functions as a major cytoskeletal organizer in ECs that orchestrates adherens junctions to control barrier function, cell migration and angiogenesis [8, 9]. It has been previously reported that VEGF induces tyrosine phosphorylation of ZO-1 and reduces expression levels of the plasma membrane protein occludin. This disrupts the localization of ZO-1 at cell junctions and increases the permeability of EC monolayers [10, 11]. Furthermore, we previously identified ZO-1 as being at the center of a signaling nexus essential for VEGF-induced proliferation of ECs during angiogenesis [12].

Zonal occludens proteins(ZO-1, ZO-2 and ZO-3) are part of the membrane-associated guanylate kinase (MAGUK) family of proteins and consists of three PDZ domains, a SH3 domain, and a guanylate kinase (GUK) domain [13, 14]. They interact with each other through binding of their corresponding PDZ-2 domains [15, 16]. ZO-1 also interacts with several membrane proteins, including claudins and JAM-A via the PDZ-1 and PDZ-2 domains, respectively, and occludin through the GUK domain [17–19]. Moreover, ZO-1 interacts with cytoplasmic proteins such as the actin-binding proteins cortactin, α-catenin and the Ras target AF6/afadin as well as the actin- and myosin-binding proteins cingulin and Shroom [9, 13, 20–22]. In addition to its roles at cell junctions, ZO-1 is also involved in transcriptional modulation through its association with the ZO-1-associated nucleic acid-binding protein (ZONAB/YB-3) to influence cell proliferation [23–26]. Once released from ZO-1, ZONAB can accumulate in the nucleus where it associates with the cell division kinase (CDK) 4 and promotes cell proliferation [24].

ECs are exposed to numerous stresses emanating from their milieu. These include reactive oxygen species (ROS), oxidized LDL, hypoxic conditions, and turbulent blood flow. The disorganized vascularity of solid tumors causes them to exhibit high levels of tissue hypoxia, which can increase cellular ROS and cause ER stress [27–30]. mTOR signaling has been shown to mediate the induction of EC survival by VEGF and angiogenesis by unconventional engagement of the unfolded protein response (UPR) pathway, independently of endoplasmic reticulum stress [31]. Stress granules (SGs) are specialized cytoplasmic structures formed in response to cellular stress that are thought to function as sites of mRNA triage, wherein individual mRNAs are dynamically sorted for storage, degradation, or translation during stress [32]. SG assembly is triggered upon exposure of cells to various stresses including heat shock, oxidative stress, hyperosmolarity, UV irradiation and viral infection [33, 34]. SGs contain many RNA-binding proteins (RBPs), such as G3BP1, TIA-1, and Y-box Binding Protein 1 (YB-1) [33, 35–37]. YB-1 is a DNA/RNA-binding protein that regulates transcription, translation, DNA repair and SG formation in part by translationally activating G3BP1 [35, 38].

The function of ZO-1 is governed by its association to numerous transmembrane, cytoplasmic, and cytoskeletal proteins. Herein, we determine the ZO-1 interactome and identify novel interactions between ZO-1 and RBPs that are constituents of SGs. We report that downregulation of ZO-1 in ECs increases SG formation and is protective against cellular stresses during angiogenesis and show that this occurs in YB-1-dependent manner.

Results

Proteomic profiling of the ZO-1 protein interactome

To determine the protein interactome of ZO-1 in ECs, bovine aortic endothelial cells (BAECs) were treated with VEGF or a vehicle, followed by ZO-1 immunoprecipitation and LC-MS/MS analyses (Supplemental Fig. S1a). In total, we identified 131 proteins as putative ZO-1 interacting proteins; of these, 60 of which were affected by the VEGF treatment (Fig. 1a). Specifically, VEGF treatment increased the interaction of ZO-1 with 59 proteins and decreased its interaction with one protein (BTF3) (Fig. 1a, Table S1, Supplemental Fig. S1b). A protein-protein interaction network was generated, and proteins were grouped based on their function as determined by Uniprot database or by Gene Ontology (GO) enrichment analyses (Fig. 1b). As expected, we found that ZO-1 interacts with cell-cell junction and cytoskeleton organization proteins such as ZO-2 (*TJP2*), gap junction protein-1 (*GJA1*), desmoplakin (*DSP*), cingulin (*CGNL1*) and junction plakoglobin (*JUP*), drebrin-1 (*DBN1*), myosin proteins (*MYL1/6, MYH11*) (Fig. 1b) [3, 22, 39–45]. Even though many of the identified ZO-1 partners were not previously reported, our MS results confirmed interactions of ZO-1 with JUP, ZO-2, Cingulin and ZONAB (*YBX3*) (Fig. 1b) [18, 24, 46]. We confirmed by immunoprecipitation the ZO-1/JUP and ZO-1/ZONAB interactions and showed that VEGF treatment increased the association between ZO-1 and JUP (Fig. 1b, c). However, VEGF decreased the ZO-1/ZONAB interaction, which was not detected by mass spectrometry (Fig. 1b, Supplemental Fig. S1c).

ZO-1 interacts with RBPs involved in stress granule formation

GO term enrichment analyses of ZO-1 interacting proteins revealed that many are RBPs involved in ribonucleoprotein complex (GO:1990904), RNA binding (GO:0003723) RNA processing (GO:0006396) and translation (GO:0006412) (Fig. 1b, d, Supplemental Fig S1d, e). We found 55 RBPs as ZO-1 interactors and VEGF treatment increased the interaction of ZO-1 with 25 of them (Table S1). We validated the interactions of ZO-1 with AIMP1 and RPL23A by performing ZO-1 immunoprecipitations (Fig. 1c). These to date unprecedented associations between ZO-1 and RBPs prompted us to compare the proteomics data of the ZO-1 interactome with those we have obtained previously for the b-catenin interactome, another cytosolic junctional protein (Table S2). Although, 42% of the 131 ZO-1 interacting proteins are RBPs, only 18% of the 62 b-catenin interactors are RBPs. Furthermore, only 3 RBPs are common to the b-catenin and ZO-1 interactomes (PPIA, RPL11 and RPS27A) (Table S2). This low abundance of RBPs in the b-catenin interactome strongly suggests that the interactions we uncovered between ZO-1 and RBPs are specific.

Interestingly, we noted that 22 ZO-1 interacting RBPs, that are part of the ribonucleoprotein complex GO term (GO:1990904), are also annotated in the RNA Granule Database (http://rnagranuledb.lunenfeld.ca/) as proteins associated with stress granules (SGs) (Fig. 1e) [47]. For instance, we identified YB-1 (*YBX1*) and FUS, known to be implicated in SGs formation in cells under stress conditions, as novel ZO-1-associated proteins [35, 48] (Fig. 1b, e). Hence, defining the ZO-1 protein interactome revealed a novel link between ZO-1 and a network of RBPs involved in SGs formation.

ZO-1 expression levels modulate stress granule formation in ECs

To investigate the link between ZO-1 and SG-related proteins, we performed siRNA-mediated depletion of ZO-1 and monitored SGs formation following exposition of ECs to stresses. ZO-1-depleted human umbilical vein endothelial cells (HUVECs) or BAECs had marked increase in SG formation in response to arsenite treatment relative to control (Fig. 2a, b; Supplemental Fig. S2a, b). Downregulation of ZO-1 increased both the percentage of ECs that exhibited G3BP1- positive SGs and the number of SGs per cell in response arsenite treatment. Of note, ZO-1 depletion did not induce SG formation in control non-stressed ECs (Fig. 2a; Supplemental Fig. S2a). Similar to arsenite treatment, SG formation in response to heat shock (42°C) significantly increased in ZO-1 downregulated ECs (Supplemental Fig. S2c, d). Additionally, SG formation was increased in arsenite-treated in hTERT-immortalized human aortic ECs (TeloHAECs) where ZO-1 was deleted using CRISPR/Cas9 compared to wildtype TeloHAECs (Supplemental Fig. S2e). Conversely, overexpression of ZO-1 in BAECs by transfection of myc-tagged ZO-1 reduced the percentage of cells with SGs in response to arsenite treatment compared to mock transfected cells (Fig. 2c). These results indicate that cellular ZO-1 expression levels are negatively correlated with SGs formation following exposure of ECs to stress conditions.

Next, we investigated whether downregulation of other cell junction proteins also resulted in increased SGs formation. In contrast to downregulation of ZO-1, siRNA-mediated depletion of VE-cadherin or b-catenin did not increase SGs formation in response to arsenite (Fig. 2d, e, Supplemental Fig. S2f). Nonetheless, knockdown of VE-cadherin or b-catenin in combination with the knockdown of ZO-1 showed a significant increase in SG formation (Fig. 2d, e). This indicates that downregulation of ZO-1 acts independently of other cell junction proteins to increase the formation of SGs in response to stress. Furthermore, downregulation of ZO-1 in sparsely plated ECs still increased SGs formation in response to arsenite treatment indicating that cell-cell contacts between ECs are not necessary for these effects of ZO-1 depletion on SG formation (Supplemental Fig. S2g, h).

ZO-1 protein levels are decreased upon exposure of ECs to stress

Since our results show that ZO-1 interacts with a subset of RBPs associated with SGs, we examined if ZO-1 and G3BP1 were colocalized in HUVECs treated with arsenite. Arsenite treatments were performed in confluent or in sparsely plated HUVECs (Fig. 2f, g). In untreated confluent ECs, the vast majority of ZO-1 localized at cell-cell junctions and G3BP1 was diffusely present in the cytoplasm. In arsenite treated ECs, levels of ZO-1 at cell junctions decreased and the presence of ZO-1 in the cytoplasm slightly increased. As expected, arsenite induced G3BP1 localization to SGs (Fig. 2f). However, in both conditions there was no detectable colocalization between ZO-1 and G3BP1 (Pearson's colocalization coefficient ZO-1/G3BP1 = 0.036). In absence of cell-cell junction in sparsely plated HUVECs, no colocalization was observed in untreated and arsenite-treated ECs even though ZO-1 was mostly observed in the cytoplasm (Pearson's colocalization coefficient ZO-1/G3BP1 = 0,0068) (Fig. 2g).

The apparent decrease in the cellular levels of ZO-1 in arsenite-treated ECs (Fig. 2f, g) prompted us to quantify the effect of various stress conditions on ZO-1 protein levels by immunoblotting. ECs were treated, in dose dependent manner, with arsenite, hydrogen peroxide or thapsigargin. We found that all three treatments markedly decreased ZO-1 expression but did not affect the levels of VE-cadherin or β-catenin (Fig. 3a-c). In addition, ZO-1 levels were significantly reduced after only 30 min of arsenite treatment (500 μM) (Fig. 3d). Because of this rapid effect of arsenite treatment on ZO-1 levels, we investigated whether ZO-1 protein degradation is proteasome-mediated. We found that inhibiting the proteosome using MG132 attenuated the arsenite-induced reduction of ZO-1 protein levels (Fig. 3e). These results suggest that exposures of ECs to stresses provoke a rapid proteasome-mediated degradation of ZO-1. Moreover, the stress-induced reduction in ZO-1 levels correlates with SG formation in ECs.

Downregulation of ZO-1 protects ECs against stress conditions

Cells form SGs to conserve energy during periods of stress [33] and reduction in ZO-1 levels increase SG formation, we thus investigated if downregulation of ZO-1 protects against cell death. We found that the

downregulation of ZO-1 decreased caspase-3 cleavage and protected ECs against cell death induced by arsenite treatment (Fig. 4a, b, Supplemental Fig. S3a). Notably, similar results were found in sparsely plated ECs, thus suggesting that these effects occur in the absence of cell-cell junctions (Supplemental Fig. S3b). In sharp contrast, downregulation of VE-cadherin or b-catenin did not protect ECs from arsenite-induced death and did not prevent the cleavage of caspase-3 (Fig. 4a, b, Supplemental Fig. S3a). Noteworthy, downregulation of VE-cadherin resulted in decreased viability of untreated ECs. Furthermore, downregulation of ZO-1 in VE-cadherin or b-catenin downregulated cells also protected cells against death induced by arsenite (Supplemental Fig. S3c). Overall, these results indicate that a reduction of ZO-1 expression levels protects ECs against stress conditions.

Next, we examined whether SG formation is modulated during the migration process of ECs. To do so, we performed 2D wound healing assays on confluent HUVEC monolayers transfected with control or ZO-1 siRNA. These experiments revealed that in migrating control-transfected ECs exposed to arsenite, cells at the leading edge have more SGs and express less ZO-1 protein than following cells located behind (Fig. 4c-e). Downregulation of ZO-1 in arsenite-treated and migrating ECs increased the percentage of cells with SGs in following cells without increasing further SGs in cells at the leading edge (Fig. 4c, d). Interestingly, downregulation of ZO-1 significantly increased migration of untreated ECs compared to control-transfected cells (Fig. 4f, g). Arsenite treatment of control-transfected cells decreased the migration of ECs and this inhibitory effect of arsenite on EC migration was absent in ZO-1 downregulated ECs (Fig. 4f, g). These results suggest that downregulation of ZO-1 promotes SG formation which in turn protects ECs from exogenous stresses that may occur during angiogenesis.

Stress conditions decrease the interaction between ZO-1 and YB-1

To identify the mechanism by which ZO-1 affects SG formation in ECs, we focussed our attention on YB-1. YB-1 is a component of SGs and a member of the Y-box factor family that includes ZONAB (also known as YB-3). ZONAB is a known ZO-1 interacting protein that we also identified, along with YB-1, in the ZO-1 interactome [35, 49, 50]. We therefore examined the effect of arsenite treatment on YB-1 levels in ECs. Consistent with its role in SG formation, YB-1 protein levels were increased in ECs treated with arsenite while the levels of ZONAB and of ZO-1 were decreased (Fig. 5a). Notably, the expression levels of YB-1 and phosphorylation of YB-1 at Ser102, a marker of transcriptional activation[51], were increased in ZO-1-downregulated ECs (Supplemental Fig. S4a). In turn, overexpression of ZO-1 in ECs resulted in decreased levels of YB-1 and pYB-1 (Supplemental Fig. S4b). Next, we examined the effect of arsenite treatment on the association between ZO-1 and YB-1 in ECs. YB-1 and ZO-1 co-immunoprecipitated from lysates of non-treated BAECs and this interaction was decreased by arsenite treatment (Fig. 5b, c).

We then examined the importance of YB-1 for SG formation in ZO-1 depleted ECs. Firstly, ZO-1 depletion in arsenite-treated HUVECs increased the percentage of cells containing SGs that were YB-1 and G3BP1 positive (Fig. 5d). Downregulation of YB-1 in ECs markedly reduced the formation of SGs induced by arsenite treatment (Fig. 5d). Furthermore, depletion of YB-1 prevented the increase in SG formation in ZO-

1-depleted cells (Fig. 5e). These results prompted us to hypothesize that downregulation of ZO-1 may promote the interaction between YB-1 and G3BP1. We show that the coimmunoprecipitation of YB-1 and G3BP1 was increased by arsenite treatment of ECs and that downregulation of ZO-1 increased the interaction between YB-1 and G3BP1 in untreated ECs (Fig. 5f). This interaction was not increased further by arsenite treatment. This suggests that ZO-1 may be restraining YB-1 from interacting with G3BP1 and that downregulation of ZO-1 expression promotes the interaction between YB-1 and G3BP1, and consequently increases SG formation in response to stress.

YB-1 is necessary for the cytoprotective effects of ZO-1 downregulation

We have shown that downregulation of ZO-1 protected ECs against cell death (Fig. 4a, b) and enhanced cell migration (Fig. 4f, g) induced by arsenite treatment. Hence, we examined the role of YB-1 in these cytoprotective effects. Downregulation of YB-1 alone did not affect the induction of cell death by arsenite treatment (Fig. 6a). However, in contrast to ZO-1 depleted cells that were protected from arsenite-induced death, simultaneous downregulation of both YB-1 and ZO-1 abolished the protective effects provided by downregulation of ZO-1 alone (Fig. 6a). Similarly, in wound healing migration assays, downregulation of YB-1 alone inhibited migration of untreated ECs, which is in sharp contrast to the increased migration seen in ZO-1 depleted ECs (Fig. 6b). Downregulation of YB-1 resulted in a more potent inhibition of migration by arsenite compared to control-treated ECs. While arsenite treatment did not inhibit the migration of ZO-1-downregulated ECs, the inhibitory effects of arsenite were restored in cells in which both ZO-1 and YB-1 were depleted (Fig. 6b). These results show that YB-1 is necessary for the protective effects against stress that are induced by the downregulation of ZO-1 in ECs.

Finally, to assess whether ZO-1 levels in ECs are regulated during angiogenesis *in vivo*, we examined the vasculature of mouse retinas at postnatal day 7, where the outward growth of the vascular plexus is incomplete. We found that ZO-1 levels were reduced in ECs located at the extremities of developing vessels, which includes tip-cells, compared to ECs located in the median portion of the retinal vasculature (Fig. 6c, d). Importantly, we found that the extremities of growing retinal vessels contained markedly more ECs with YB-1 and G3BP1 positive SGs than vessels located in the median portion of the retinal vasculature (Fig. 6e, f; Supplemental Fig. S5). Altogether these results corroborate a model whereby ZO-1 downregulation leads to protection of ECs under stress and show that this is at least in part mediated by YB-1-dependent SG formation.

Discussion

The junction protein ZO-1 links transmembrane proteins with cortical actin cytoskeletal proteins and this is instrumental in assembling cell junctions[8]. Herein, we reveal that, in addition to its roles at cell junctions and to the ZONAB-dependent function in transcription, ZO-1 has a major impact on the fate of ECs under stress and during angiogenesis. Indeed, we show that in ECs ZO-1 is a negative regulator of

SGs formation through its association with YB-1 and that ZO-1/YB-1 interactions regulate cytoprotection against exposure of cells to stresses.

By defining the VEGF-regulated ZO-1 interactome, we found that in ECs ZO-1 interacts with RBPs and in particular with proteins that are part of stress granules. This suggested that ZO-1 may act as a regulator of SGs formation. Downregulation of ZO-1 led to increased SGs formation following stress and we showed that exposure of ECs to stress decreased ZO-1 protein levels. Furthermore, ECs with reduced ZO-1 expression were more resistant to arsenite-induced cell death. This suggested that ECs decrease ZO-1 expression to promote SG formation and to be protected from stresses. We also revealed that actively migrating ECs or ECs located at the tip of developing vessels of the mouse retina expressed less ZO-1 and exhibited more SGs. Importantly, the induction of SG formation and the cytoprotective effects of ZO-1 downregulation were dependent on the expression of YB-1, an RBP involved in SG assembly, which we found to be a novel ZO-1 associated protein [35–37, 52].

YB-1 is part of the Y-box family of proteins that also includes YB-2 and ZONAB/YB-3. ZONAB is a known ZO-1-associated protein whose transcriptional activity is regulated by ZO-1 and involved in contact inhibition of proliferation [23–26]. The identification of another Y-box protein associated to ZO-1 suggests that the cold shock domains present in this protein family may be involved in the association with ZO-1 [50, 53, 54]. In conjunction with SG formation and to minimize cellular damage during stress, the translation of the great majority of mRNA is attenuated [55–57]. However, some stress-responsive mRNAs containing upstream open reading frames (uORFs), such as ATF4 mRNA, are translationally activated under stress conditions [58, 59]. Notably, YB-1 has been implicated in the stress specific translation of some mRNAs involved in the angiogenic process, including HIF1α and VEGF [53, 60, 61]. Hence, this suggests that ZO-1, in association with YB-1 or with other RBPs involved in translation, may also be a component of translational regulation of stress-regulated mRNAs. The identification of a significant amount of RBPs in the ZO-1 interactome, with many of these associations regulated by VEGF, highlights the multifunctional role for ZO-1 in cells. Interestingly, ZO-1 is present in datasets from recent studies that identified the RNA-binding proteome [62, 63].

Herein, we provide the first evidence that SG formation in ECs is involved in angiogenesis and demonstrate that expression levels of ZO-1 regulate this process. The presence of G3BP1 and YB-1 positive SGs in ECs, which have reduced ZO-1 expression, at the tip of the developing vasculature of the mouse retina revealed an important role for SGs in angiogenesis. Levels of ZO-1 are actively regulated and have been shown to determine cell proliferation and differentiation as well as the invasiveness potential of malignant cells [12, 23, 24]. In summary, the ZO-1 interactome revealed a link between ZO-1 and YB-1. This interaction regulates SGs formation and revealed a new role for ZO-1 in controlling the fate of ECs under stress, which contributes to the regulation of vascular homeostasis and angiogenesis.

Methods

Cell culture and treatments

Bovine aortic endothelial cells (BAECs) obtained from VEC Technologies (Rensselaer, NY, USA) were cultured in Dulbecco Modified Eagle Medium (DMEM, Thermo Fisher, Waltham, MA, USA) supplemented with 10% fetal bovine serum (HyClone, GE Healthcare Life Sciences, Pistacaway, NJ, USA), 2 mM L-glutamine, 100 U/ml penicillin, and 100 µg/ml streptomycin (Thermo Fisher). Human umbilical vein endothelial cells (HUVECs) obtained from VEC Technologies were cultured in M199 media supplemented with 20% FBS, 2 mM L-glutamine, 100 U/ml penicillin, and 100 µg/ml streptomycin and Endothelial Cell Growth Supplement (ECGS, Corning Life Sciences, Corning, NY, USA). Recombinant human VEGF-A was obtained from R&D System (Minneapolis, MI, USA). Sodium arsenite ($NaAsO_2$), hydrogen peroxide H_2O_2 and MG-132 were from Millipore-Sigma (Burlington, MA, USA) and Thapsigargin was from Alomone labs (Jerusalem, Israel). Before each treatment, BAECs and HUVECs were serum starved for 6 hrs followed by a treatment. The doses and the duration of treatments are specified in the figure legends.

Cell migration and viability assays

Cell migration was measured in a wound healing assay. Briefly, BAECs plated in 6-well plates were transfected with siRNAs and allowed to reach 90% confluency over 48 hrs. Scratches on the monolayer were performed with a 200-µl pipette tip. Images of the wounded area were taken using a Zeiss Axio-Observer Z1 epifluorescent microscope (2.5×) at the beginning (t=0) and after 16 hrs of migration. Wound closure was measured using the draw spline contour tool on Zen Blue.

Cell viability was determined by Trypan blue exclusion. Viable cells were manually counted using an hemacytometer or using a Countess III cell counter (Life Technologies).

Plasmids and transfections

ZO-1, YB-1, β-catenin and VE-cadherin small interfering RNA (siRNA) as well as non-silencing control siRNA were obtained from Horizon Discoveries (Chicago, IL, USA). siCT AUG AAC GUG AAU UGC UCA AUU, siVE-cadherin (bovine) ACA AAG AAC UGG ACA GAG AUU, siVE-cadherin (human) GCA CAU UGA UGA AGA GAA A, siZO-1 (bovine) GCA GAG AGG AAG AGA GAA UUU, siZO-1 (human) UGG AAA UGA UGU UGG AAU A, siβ-catenin (human) CCA CUA AUG UCC AGC GUU U, siYB-1 (bovine) CAG CAG AAC UAC CAG AAU A, siYB-1 (human) CGG CAA UGA AGA AGA UAA A. BAECs and HUVECs were transfected with plasmids or siRNAs using Lipofectamine 2000 (Thermo Fisher) according to manufacturer's instructions.

Immunoblotting and immunoprecipitation

Cells were solubilized with a lysis buffer containing 1% Nonidet P-40, 0.1% sodium dodecyl sulfate (SDS), 0.1% deoxycholic acid, 50 mM Tris (pH 7.4), 0.1 mM EGTA, 0.1 mM EDTA, 50 mM NaCl, 20 mM NaF, 1 mM $Na_4P_2O_7$ and 1 mM Na_3VO_4. Lysate were incubated for 30 minutes at 4°C, centrifuged at 14000 g for 10 minutes and boiled in SDS sample buffer. For the immunoprecipitation, BAECs were treated (with VEGF or arsenite) and were lysed in the lysis buffer with NaCl adjusted to 75 mM. The lysates were centrifuged at 20,000*g* for 10 min and 1 mg of proteins was used for immunoprecipitation with 1 µg of

antibody overnight. Immunoglobulin G (IgG) control IPs were used as a negative control. Immunocomplexes were incubated with protein A sepharose beads (Millipore-Sigma) for 1 hour, washed in lysis buffer and boiled in SDS sample buffer. The samples were separated by SDS-polyacrylamide gel electrophoresis, transferred onto a nitrocellulose membrane (Hybond-ECL, GE Healthcare Life Science), and western blotted. Detection was performed using HRP-coupled antibodies and an Image Quant LAS4000 chemiluminescence-based detection system (enhanced chemiluminescence) (GE Healthcare Life Science).

Antibodies

For immunoblots we used horseradish peroxidase (HRP)-coupled antibodies from Jackson ImmunoResearch Laboratories (West Grove, PA, USA). The primary antibodies used for immunoblots or immunofluorescence experiments were: rabbit anti-ZO-1 and mouse anti-ZO-1 (617300 and 339100, Thermo Fisher), rabbit anti-MYC-Tag (2278S), rabbit anti-phospho-Ser102-YB1 (2900S), rabbit-anti-YB1 (4202S for Immunofluorescence, 9744S for Immunoblotting), rabbit anti-caspase-3 (9665T) and mouse anti-actin (3700S) (New England Biolabs, Ipswich MA, USA), mouse anti-G3BP1 (611126) and mouse anti-β-catenin (610153) (BD Biosciences, San Jose, CA, USA) goat anti-VE-cadherin (R&D Systems), mouse anti-EMAP II/AIMP1, mouse anti-FUS, anti-Ribosomal Protein L23a (sc-517097, Santa Cruz, CA, USA) and mouse anti- γ-catenin (JUP) (610253, BD Biosciences, San Jose, CA, USA).

Sample preparation for MS

For MS experiments, immunoprecipitates were washed three times with lysis buffer and then three times detergent free lysis buffer. Then, immunoprecipitated proteins were eluted in Urea 8 M, 50 mM Tris (pH 7.4), and proteases and phosphatases inhibitors. Beads were incubated with 50 µl elution buffer at room temperature for 30 minutes with frequent agitation. Eluted proteins were reduced at 37°C using dithiothreitol (DTT) for one hour and alkylated by iodoacetamide for 60 minutes at room temperature in the dark. The mixture was digested using trypsin (ratio enzyme/total protein of 1:50) followed by incubation at 37°C overnight. The tryptic digestion was quenched by adding 1% TFA (trifluoroacetic acid). Peptides were re-solubilized under agitation for 15 minutes in 21 µL of 1% ACN / 1% formic acid. The LC column was a PicoFrit fused silica capillary column (17 cm x 75 µm i.d; New Objective, Woburn, MA), self-packed with C-18 reverse-phase material (Jupiter 5 µm particles, 300 Å pore size; Phenomenex, Torrance, CA) using a high-pressure packing cell. This column was installed on the Easy-nLC II system (Proxeon Biosystems, Odense, Denmark) and coupled to the LTQ Orbitrap Velos (ThermoFisher Scientific, Bremen, Germany) equipped with a Proxeon nanoelectrospray Flex ion source. The buffers used for chromatography were 0.2% formic acid (buffer A) and 100% ACN / 0.2% formic acid (buffer B). Peptides were loaded on-column at a flow rate of 600 nL/minute and eluted with a 2 slopes gradient at a flow rate of 250 nL/minute. Solvent B first increased from 1 to 40% in 110 minutes and then from 40 to 80% B in 50 minutes.

MS data processing

Raw mass spectrometry data were processed using the MaxQuant software (version 1.5.3.17). Database searching was performed using the Andromeda search engine (version 1.5.3.17) integrated into MaxQuant against the bovine UniProt database and against the human UniProt database. MaxQuant default parameters were used with the exception of minimum ratio count and LFQ minimum ratio count set to 1. Enzyme specificity was set to trypsin and up to two missed cleavages was allowed. Cysteine carbamidomethylation (C) was set as fixed modification and oxidation (M) and phosphorylation (STY) were set as variable modification. The minimum required peptide length was 6 amino acids. Mass tolerances for precursor ions and fragment ions were set to 20 ppm and 0.5 Da, respectively. The "matching between runs" algorithm in MaxQuant was enabled. The false discovery rate (FDR) was estimated by searching against the databases with the reversed sequences. For protein and peptide identification, the maximum FDR was set to 1%. Three independent biological replicates and two technical replicates were performed. Correlations between the biological replicates are shown in Supplemental Fig. S1b. For proteins quantification, LFQ intensity values from biological and technical replicates that represent protein abundance were used for statistical analysis. Protein identification in at least two biological replicates was required for further analysis. Also, at least two peptides of a protein must be identified to be considered as a potential ZO-1 interacting protein. LFQ intensities across different samples were first normalized according to the intensities of the bait protein ZO-1 in each sample in order to have equal amounts of ZO-1 in each replicate. Then, intensities of ZO-1 interactors across different samples were adjusted according to the normalized ZO-1 intensities in each sample. Normalized LFQ intensities were used for determination of specific protein–protein interactions.

Significant interactors were determined by performing a statistical analysis of the bait IPs of each condition versus IgG control IPs. Datasets were log2 transformed and using Perseus tools, we imputed normal distributed values for missing values using a normal distribution with width of 0.3 and a downshift of the mean by 1.8 compared to distribution of all LFQ intensities. Then, we performed a student's t-test–based comparisons of bait IPs versus IgG control IPs to identify significant interactors with false discovery threshold set at 0.05. Permutation-based FDR method in Perseus was used to perform multiple testing corrections. We calculated the average intensities of ZO-1 interacting proteins between the replicates and the treated/untreated ratio for each protein was determined. To determine the interactors that are modulated by each treatment, we compared statistically using a student's t-test the bait IPs of each condition versus control condition. Only interactors with more than 2-fold change compared to control condition were considered as affected by VEGF treatment. Interactors that are statistically influenced by VEGF treatment with a p-value<0.05 were considered significantly modulated by VEGF. The mass spectrometry proteomics data have been deposited to the ProteomeXchange Consortium via the PRIDE partner repository with the dataset identifier PXD029332 [64]. The following secure account has been created to allow review while the data remain in private status: Username: reviewer_pxd029332@ebi.ac.uk ; Password: 7qk7dVrX

Proteomics data analysis

Gene ontology annotations for biological processes were obtained from the Gene Ontology integrated in STRING database (version 11.0). Only GO annotations that were significantly enriched with a p value of less than 0.05 were used in the analysis. To generate protein interactions network, STRING interactions database was used. The published or informatic-predicted interactions were first determined using standard STRING-defined confidence (medium confidence 0.4). Protein enrichment in the protein interaction network was manually annotated based on the GO biological process enrichment. The obtained STRING network data were imported into the Cytoscape software for visualisation. For clustering analysis, The Markov Cluster Algorithm (MCL) algorithm with clusterMaker2 plugin in Cytoscape was used to identify functional protein clusters within the networks.

Immunofluorescence

BAECs and HUVECs were transfected and then cultured on 0.1% gelatin-coated coverslips. Cells were washed with cold PBS and fixed for 20 minutes in 4% paraformaldehyde (PFA) and permeabilized with 0.3% Triton X-100. Cells were rinsed with PBS and blocked with 1% BSA for 1 hour at room temperature. After blocking, cells were incubated with primary antibodies G3BP1 (dilution 1:100), ZO-1 (dilution 1:100), YB-1 (dilution 1:50) 2 hrs at room temperature in 0.1% BSA in PBS. Bound primary antibodies were visualized after 1 hour of incubation using Alexa Fluor 488-labeled donkey anti-goat, Alexa Fluor 568-labeled donkey anti-mouse, Alexa Fluor 568-labeled donkey anti-rabbit, Alexa Fluor 488 goat anti-mouse. Coverslips were mounted using Fluoromount (Millipore-Sigma) and observed using an LSM800 Zeiss confocal laser-scanning microscope (Carl Zeiss, Germany). Samples were viewed with a 63×/1.5 zoom oil objective. Images were assembled via ImageJ and Photoshop CC (Adobe Systems). Colocalization was analyzed by determining the Pearson colocalization coefficient using the Zen software (Zeiss).

Retina Immunostaining

All animal studies were approved by the Animal Care Committee of the University of Montreal in agreement with the guidelines established by the Canadian Council on Animal Care. C57BL/6J wildtype were purchased from The Jackson Laboratory (Bar Harbor, ME, USA).

Dissection and whole mount staining of postnatal retinas of mice at the stage P5 were performed as described previously[12]. Retinas were fixed for 2 hrs on ice in 4% PFA. Dissected retinas were blocked overnight in 1% BSA, 0.3% Triton X-100 in PBS. For lectin I staining, retinas were equilibrated with Pblec buffer containing 1 mm $CaCl_2$, 1 mm $MgCl_2$, 1% Triton X-100 in PBS (pH 6.8) and then stained with Rhodamine conjugated Lectin I (dilution 1:100) overnight at 4°C. For G3BP1, YB-1 or ZO-1 staining, retinas were incubated with mouse anti-G3BP1 (dilution 1:100), rabbit anti-ZO-1 (dilution 1:100) and rabbit anti-YB-1 (dilution 1:50) in blocking buffer 2 hrs at 4°C. After primary incubation, retinas were labeled with Alexa-Fluor 488-labeled goat anti-mouse or anti-rabbit (dilution 1:100). Stained retinas were flat mounted using Fluoromount G (Electron Microscopy Sciences, Hatfield, PA). Z-stack confocal imaging was performed on Zeiss LSM800 confocal laser-scanning microscope using a 63× oil objective and a 2.5× digital zoom. All quantifications were performed on z-stack confocal images. Images were analyzed using Fiji software (NIH, Bethesda, MD, USA) or the built-in tools in Zen software (Zeiss).

Quantification of SGs staining

The number of SGs was quantified using the ImageJ software. IF images were randomly taken with a 63× objective lens in 10 different fields. The plug-in “Analyze particles” was used to count the number of SGs. The percentage of cells with SGs was calculated by counting the number of cells displaying SGs divided by the total number of cells.

Statistical analyses

Data are represented as the means ± SEM. Two-tailed independent Student’s tests were used when comparing two groups. Comparisons between multiple groups were made using one-way ANOVA followed by post-hoc Bonferoni’s multiple comparisons test among groups on using Prism 5 software (GraphPad, San Diego, CA, USA). P-value < 0.05 was considered statistically significant.

Declarations

FUNDING: This work was funded by an operating grants from the Cancer Research Society of Canada and from the Canadian Institutes of Health Research (CIHR) MOP - 142180 to J.-P.G.

Author contributionS: Y.E.B. and R.C. designed and performed the experiments, analyzed the data, prepared figures, and wrote the manuscript; J.C., V.G.L. and C.D. performed experiments, analyzed data and revised the manuscript; A.C., E.L., S.A., I.T. and L.H. provided key expertise and revised the manuscript; J.-P.G. obtained funding, designed, and supervised the experiments, analyzed the data, prepared figures, and wrote the manuscript.

COMPETING INTEREST: The authors declare no competing interests.

References

1. Giannotta, M., Trani, M. & Dejana, E. VE-Cadherin and Endothelial Adherens Junctions: Active Guardians of Vascular Integrity. *Developmental Cell* **26**, 441–454 (2013).
2. Bazzoni, G. & Dejana, E. Endothelial cell-to-cell junctions: molecular organization and role in vascular homeostasis. *Physiol Rev* **84**, 869–901 (2004).
3. Wallez, Y. & Huber, P. Endothelial adherens and tight junctions in vascular homeostasis, inflammation and angiogenesis. *Biochimica et Biophysica Acta (BBA) - Biomembranes* **1778**, 794–809 (2008).
4. Vittet, D., Buchou, T., Schweitzer, A., Dejana, E. & Huber, P. Targeted null-mutation in the vascular endothelial-cadherin gene impairs the organization of vascular-like structures in embryoid bodies. *Proceedings of the National Academy of Sciences* **94**, 6273-6278 (1997).
5. Cattelino, A. *et al.* The conditional inactivation of the β-catenin gene in endothelial cells causes a defective vascular pattern and increased vascular fragility. **162**, 1111–1122 (2003).

6. Beckers, C.M.L., García-Vallejo, J.J., Van Hinsbergh, V.W.M. & Van Nieuw Amerongen, G.P. Nuclear targeting of β-catenin and p120ctn during thrombin-induced endothelial barrier dysfunction. *Cardiovascular Research* **79**, 679–688 (2008).
7. Katsuno, T. *et al.* Deficiency of zonula occludens-1 causes embryonic lethal phenotype associated with defected yolk sac angiogenesis and apoptosis of embryonic cells. *Molecular Biology of the Cell* **19**, 2465–2475 (2008).
8. Tornavaca, O. *et al.* ZO-1 controls endothelial adherens junctions, cell-cell tension, angiogenesis, and barrier formation. *Journal of Cell Biology* **208**, 821–838 (2015).
9. Tsukita, S., Furuse, M. & Itoh, M. Multifunctional strands in tight junctions. *Nature Reviews Molecular Cell Biology* **2**, 285–293 (2001).
10. Antonetti, D.A., Barber, A.J., Hollinger, L.A., Wolpert, E.B. & Gardner, T.W. Vascular Endothelial Growth Factor Induces Rapid Phosphorylation of Tight Junction Proteins Occludin and Zonula Occluden 1. *Journal of Biological Chemistry* **274**, 23463–23467 (1999).
11. Balda, M.S. & Matter, K. Tight junctions at a glance. *Journal of Cell Science* **121**, 3677–3682 (2008).
12. Chidiac, R. *et al.* Comparative phosphoproteomics analysis of VEGF and angiopoietin-1 signaling reveals ZO-1 as a critical regulator of endothelial cell proliferation. *Molecular and Cellular Proteomics* **15**, 1511–1525 (2016).
13. Matter, K. & Balda, M.S. Signalling to and from tight junctions. **4**, 225–237 (2003).
14. Perez-Moreno, M., Jamora, C. & Fuchs, E. Sticky Business. *Cell* **112**, 535–548 (2003).
15. Gumbiner, B., Lowenkopf, T. & Apatira, D. Identification of a 160-kDa polypeptide that binds to the tight junction protein ZO-1. *Proceedings of the National Academy of Sciences* **88**, 3460-3464 (1991).
16. Wu, J. *et al.* Domain-swapped dimerization of the second PDZ domain of ZO2 may provide a structural basis for the polymerization of claudins. *J Biol Chem* **282**, 35988–35999 (2007).
17. Ebnet, K. Junctional Adhesion Molecule (JAM) interacts with the PDZ domain containing proteins AF-6 and ZO-1. *Journal of Biological Chemistry* (2000).
18. Itoh, M. *et al.* Direct Binding of Three Tight Junction-Associated Maguks, Zo-1, Zo-2, and Zo-3, with the Cooh Termini of Claudins. *Journal of Cell Biology* **147**, 1351–1363 (1999).
19. Fanning, A.S., Jameson, B.J., Jesaitis, L.A. & Anderson, J.M. The Tight Junction Protein ZO-1 Establishes a Link between the Transmembrane Protein Occludin and the Actin Cytoskeleton. *Journal of Biological Chemistry* **273**, 29745–29753 (1998).
20. Katsube, T. *et al.* Cortactin Associates with the Cell-Cell Junction Protein ZO-1 in bothDrosophilaand Mouse. *Journal of Biological Chemistry* **273**, 29672–29677 (1998).
21. Schneeberger, E.E. & Lynch, R.D. The tight junction: a multifunctional complex. *American Journal of Physiology-Cell Physiology* **286**, C1213-C1228 (2004).
22. Etournay, R. *et al.* Shroom2, a myosin-VIIa- and actin-binding protein, directly interacts with ZO-1 at tight junctions. *Journal of Cell Science* **120**, 2838–2850 (2007).

23. Balda, M.S. The tight junction protein ZO-1 and an interacting transcription factor regulate ErbB-2 expression. *The EMBO Journal* **19**, 2024–2033 (2000).
24. Balda, M.S., Garrett, M.D. & Matter, K. The ZO-1-associated Y-box factor ZONAB regulates epithelial cell proliferation and cell density. *Journal of Cell Biology* **160**, 423–432 (2003).
25. Spadaro, D. *et al.* Tension-Dependent Stretching Activates ZO-1 to Control the Junctional Localization of Its Interactors. *Current Biology* **27**, 3783-3795.e3788 (2017).
26. Georgiadis, A. *et al.* The tight junction associated signalling proteins ZO-1 and ZONAB regulate retinal pigment epithelium homeostasis in mice. *PLoS ONE* **5**, 1–10 (2010).
27. Binet, F. & Sapieha, P. ER stress and angiogenesis. *Cell Metabolism* **22**, 560–575 (2015).
28. Auf, G. *et al.* Inositol-requiring enzyme 1 is a key regulator of angiogenesis and invasion in malignant glioma. *Proceedings of the National Academy of Sciences* **107**, 15553-15558 (2010).
29. Atkins, C. *et al.* Characterization of a Novel PERK Kinase Inhibitor with Antitumor and Antiangiogenic Activity. *Cancer Research* **73**, 1993–2002 (2013).
30. Ghosh, R. *et al.* Transcriptional Regulation of VEGF-A by the Unfolded Protein Response Pathway. *PLoS ONE* **5**, e9575 (2010).
31. Karali, E. *et al.* VEGF Signals through ATF6 and PERK to promote endothelial cell survival and angiogenesis in the absence of ER stress. *Mol Cell* **54**, 559–572 (2014).
32. Protter, D.S.W. & Parker, R. Principles and Properties of Stress Granules. *Trends in cell biology* **26**, 668–679 (2016).
33. Anderson, P. & Kedersha, N. Visibly stressed: the role of eIF2, TIA-1, and stress granules in protein translation. *Cell Stress Chaperones* **7**, 213–221 (2002).
34. McCormick, C. & Khaperskyy, D.A. Translation inhibition and stress granules in the antiviral immune response. *Nature Reviews Immunology* **17**, 647–660 (2017).
35. Somasekharan, S.P. *et al.* YB-1 regulates stress granule formation and tumor progression by translationally activating G3BP1. *Journal of Cell Biology* **208**, 913–929 (2015).
36. Youn, J.-Y. *et al.* High-Density Proximity Mapping Reveals the Subcellular Organization of mRNA-Associated Granules and Bodies. *Molecular Cell* **69**, 517-532.e511 (2018).
37. Markmiller, S. *et al.* Context-Dependent and Disease-Specific Diversity in Protein Interactions within Stress Granules. *Cell* **172**, 590-604.e513 (2018).
38. El-Naggar, A.M. & Sorensen, P.H. Translational control of aberrant stress responses as a hallmark of cancer. *J Pathol* **244**, 650–666 (2018).
39. Dejana, E. Endothelial cell–cell junctions: happy together. *Nature Reviews Molecular Cell Biology* **5**, 261–270 (2004).
40. Sourisseau, T. *et al.* Regulation of PCNA and Cyclin D1 Expression and Epithelial Morphogenesis by the ZO-1-Regulated Transcription Factor ZONAB/DbpA. *Molecular and Cellular Biology* **26**, 2387–2398 (2006).

41. Cordenonsi, M. *et al.* Cingulin Contains Globular and Coiled-Coil Domains and Interacts with Zo-1, Zo-2, Zo-3, and Myosin. *Journal of Cell Biology* **147**, 1569–1582 (1999).
42. Nagasawa, K. *et al.* Possible involvement of gap junctions in the barrier function of tight junctions of brain and lung endothelial cells. *Journal of Cellular Physiology* **208**, 123–132 (2006).
43. Nyqvist, D., Giampietro, C. & Dejana, E. Deciphering the functional role of endothelial junctions by using in vivo models. *EMBO reports* **9**, 742–747 (2008).
44. Schossleitner, K. *et al.* Evidence That Cingulin Regulates Endothelial Barrier Function In Vitro and In Vivo. *Arteriosclerosis, Thrombosis, and Vascular Biology* **36**, 647-654 (2016).
45. Ambrosi, C. *et al.* Connexin43 Forms Supramolecular Complexes through Non-Overlapping Binding Sites for Drebrin, Tubulin, and ZO-1. *PLOS ONE* **11**, e0157073 (2016).
46. D'Atri, F., Nadalutti, F. & Citi, S. Evidence for a Functional Interaction between Cingulin and ZO-1 in Cultured Cells. *Journal of Biological Chemistry* **277**, 27757–27764 (2002).
47. Youn, J.-Y. *et al.* Properties of Stress Granule and P-Body Proteomes. *Molecular Cell* **76**, 286–294 (2019).
48. Sama, R.R.K. *et al.* FUS/TLS assembles into stress granules and is a prosurvival factor during hyperosmolar stress. *Journal of Cellular Physiology* **228**, 2222–2231 (2013).
49. Eliseeva, I.A., Kim, E.R., Guryanov, S.G., Ovchinnikov, L.P. & Lyabin, D.N. Y-box-binding protein 1 (YB-1) and its functions. *Biochemistry (Moscow)* **76**, 1402–1433 (2011).
50. Mordovkina, D. *et al.* Y-Box Binding Proteins in mRNP Assembly, Translation, and Stability Control. *Biomolecules* **10** (2020).
51. Sutherland, B.W. *et al.* Akt phosphorylates the Y-box binding protein 1 at Ser102 located in the cold shock domain and affects the anchorage-independent growth of breast cancer cells. *Oncogene* **24**, 4281–4292 (2005).
52. Guarino, A.M. *et al.* YB-1 recruitment to stress granules in zebrafish cells reveals a differential adaptive response to stress. *Scientific Reports* **9**, 1–14 (2019).
53. Coles, L.S. *et al.* A multi-protein complex containing cold shock domain (Y-box) and polypyrimidine tract binding proteins forms on the vascular endothelial growth factor mRNA: Potential role in mRNA stabilization. *European Journal of Biochemistry* **271**, 648–660 (2004).
54. Lindquist, J.A. & Mertens, P.R. Cold shock proteins: From cellular mechanisms to pathophysiology and disease. *Cell Communication and Signaling* **16**, 1–14 (2018).
55. Shenton, D. *et al.* Global translational responses to oxidative stress impact upon multiple levels of protein synthesis. *Journal of Biological Chemistry* **281**, 29011–29021 (2006).
56. Pakos-Zebrucka, K. *et al.* The integrated stress response. *EMBO reports* **17**, 1374–1395 (2016).
57. Mateju, D. *et al.* Single-Molecule Imaging Reveals Translation of mRNAs Localized to Stress Granules. *Cell* **183**, 1801-1812.e1813 (2020).
58. Vattem, K.M. & Wek, R.C. Reinitiation involving upstream ORFs regulates ATF4 mRNA translation in mammalian cells. *Proceedings of the National Academy of Sciences* **101**, 11269-11274 (2004).

59. Roybal, C.N., Hunsaker, L.A., Barbash, O., Jagt, D.L.V. & Abcouwer, S.F. The Oxidative Stressor Arsenite Activates Vascular Endothelial Growth Factor mRNA Transcription by an ATF4-dependent Mechanism. *Journal of Biological Chemistry* **280**, 20331–20339 (2005).
60. El-Naggar, A.M. *et al.* Translational Activation of HIF1α by YB-1 Promotes Sarcoma Metastasis. *Cancer Cell* **27**, 682–697 (2015).
61. Evdokimova, V., Ovchinnikov, L.P. & Sorensen, P.H.B. Y-box Binding Protein 1: Providing a New Angle on Translational Regulation. *Cell Cycle* **5**, 1143–1147 (2006).
62. Queiroz, R.M.L. *et al.* Comprehensive identification of RNA–protein interactions in any organism using orthogonal organic phase separation (OOPS). *Nature Biotechnology* **37**, 169–178 (2019).
63. Trendel, J. *et al.* The Human RNA-Binding Proteome and Its Dynamics during Translational Arrest. *Cell* **176**, 391-403.e319 (2019).
64. Perez-Riverol, Y. *et al.* The PRIDE database and related tools and resources in 2019: improving support for quantification data. *Nucleic Acids Research* **47**, D442-D450 (2019).

Figures

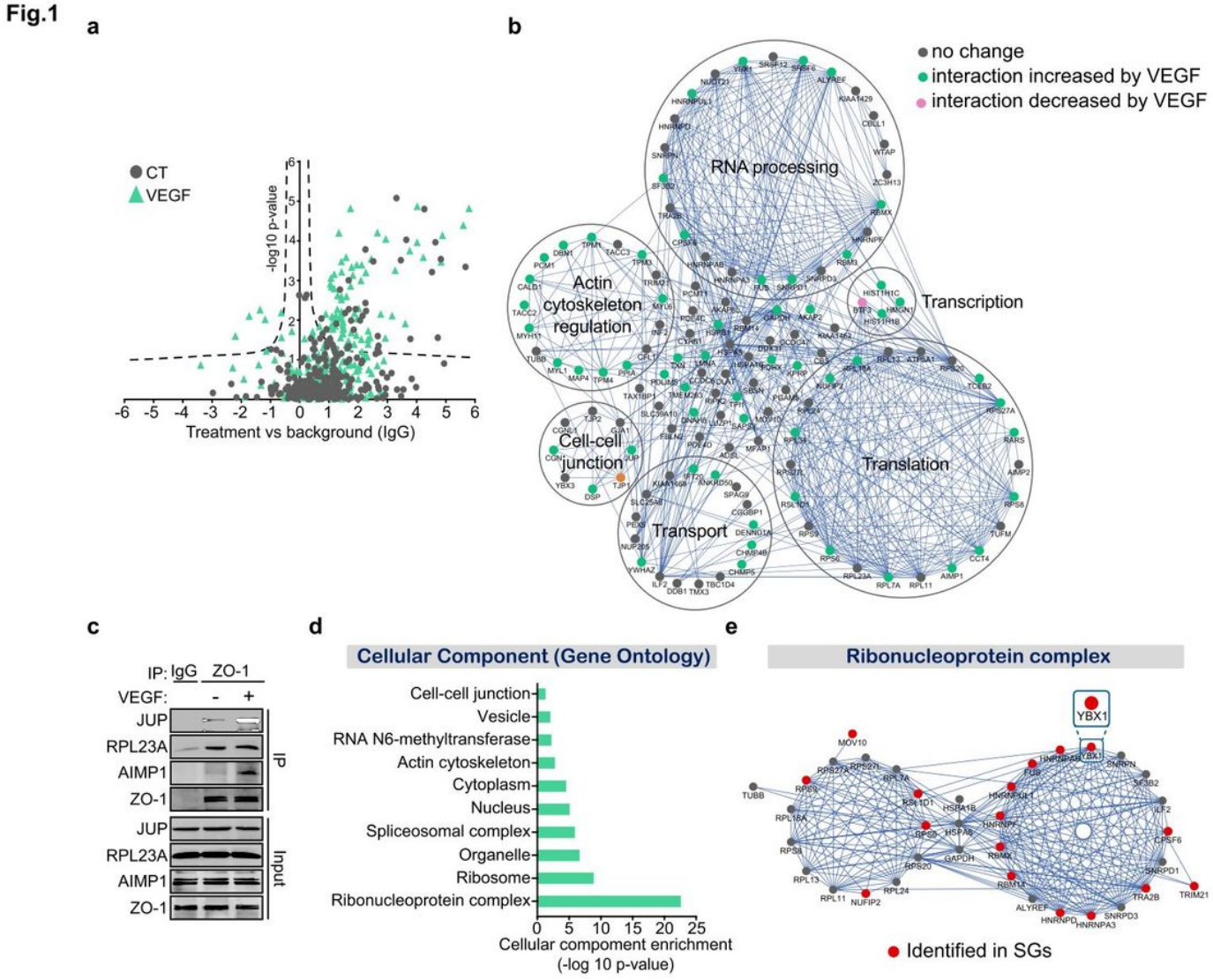

Figure 1

Proteomic analysis of the ZO-1 interactome in endothelial cells.

a, Volcano plot showing the distribution of proteins abundance of control (CT) and VEGF treated conditions over IgG control (fold-change, x axis) as a function of statistical significance (-log10 of p-value, y axis). The hyperbolic curves indicate a false discovery rate (FDR) cutoff of 0.05 and separates specific from non-specific interactors. Every point represents one protein. **b**, Protein interaction network of ZO-1 (TJP1, orange) interacting proteins using STRING database and visualized by Cytoscape. The functional enrichment was manually annotated using GO terms of the biological process category and Uniprot database. Green corresponds to ZO-1 associated proteins that were increased by VEGF treatment. Pink corresponds to ZO-1 associated proteins that were decreased by VEGF treatment. **c,** Proteins were immunoprecipitated using ZO-1 antibody from whole lysates of BAEC treated or not with VEGF (40 ng/ml, 10 min). Then, interacting proteins were detected by immunoblot using specific antibodies against ZO-1, JUP, AIMP1 and RPL23A proteins. Non-immune IgG serves as control for non-specific co-immunoprecipitation. **d,** Enrichment analysis for GO cellular component terms of ZO-1 interacting

proteins. **e,** Ribonucleoprotein complex interaction network. Protein interaction network of ZO-1 interacting proteins part of the ribonucleoprotein complex GO term (GO:1990904). Red corresponds to proteins associated with stress granules (SGs).

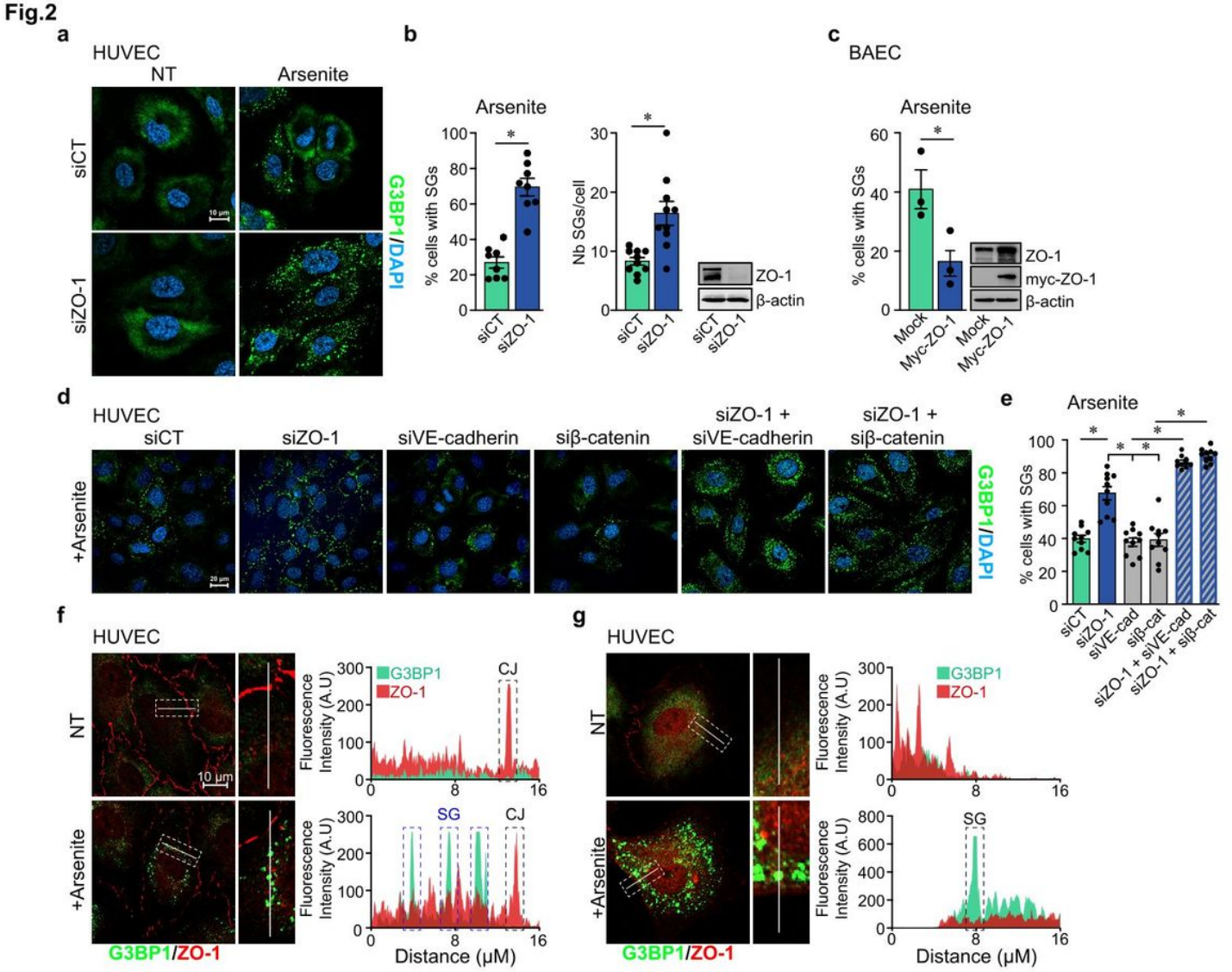

Figure 2

ZO-1 depletion increases SG formation in ECs.

a, Increased SG formation in ZO-1 depleted cells. Immunofluorescence staining of SGs using antibodies against G3BP1 in siCT and siZO-1 transfected HUVECs in absence (NT) or presence of sodium arsenite (500 µM for 30 min). Nuclei are stained with DAPI. **b,** Quantification of G3BP1 positive SGs shown in (a). The percentage of cells with SGs (left) or the number of SGs per cell (right) was calculated in 8 fields from 3 independent experiments. The downregulation efficiency of siRNA was confirmed by western blot. **c,** Overexpression of ZO-1 decreases SG formation. BAECs expressing myc-ZO-1 were treated with arsenite (500 µM; 30 min) and the percentage of cells with SGs (G3BP1) was quantified. Results are from at least fifty myc-positive cells per condition in three independent experiments. The expression of myc-

ZO-1 plasmid was confirmed by western blot. **d,** Increased SG formation is specific to downregulation of ZO-1. Immunofluorescence staining of SGs in HUVECs transfected with siRNA against ZO-1, VE-cadherin, siβ-catenin or ZO-1 and VE-cadherin or ZO-1 and β-catenin and treated or not with arsenite **e,** Quantification of the percentage of cells with G3BP1 positive SGs shown in (**d**). Cells with SGs were calculated in ten 40X fields per condition in three independent experiments. Efficacy of siRNA-mediated knockdowns are shown in Supplemental Fig. S2f. **f, g,** ZO-1 does not localize in SGs of confluent or sparse ECs. Immunofluorescence staining of ZO-1 and G3BP1 in confluent (**f**) or sparsely (**g**) plated HUVECs treated or not with arsenite (500 μM; 30 min). Fluorescence intensities of ZO-1 (red) and G3BP1 (green) in HUVECs along the white lines are represented as arbitrary units (A.U.). Fluorescence intensities across stress granules (SG) and cell junctions (CJ) is indicated. **b, c, d, e,** Data are represented as mean ± SEM; * p<0.05.

Fig.3

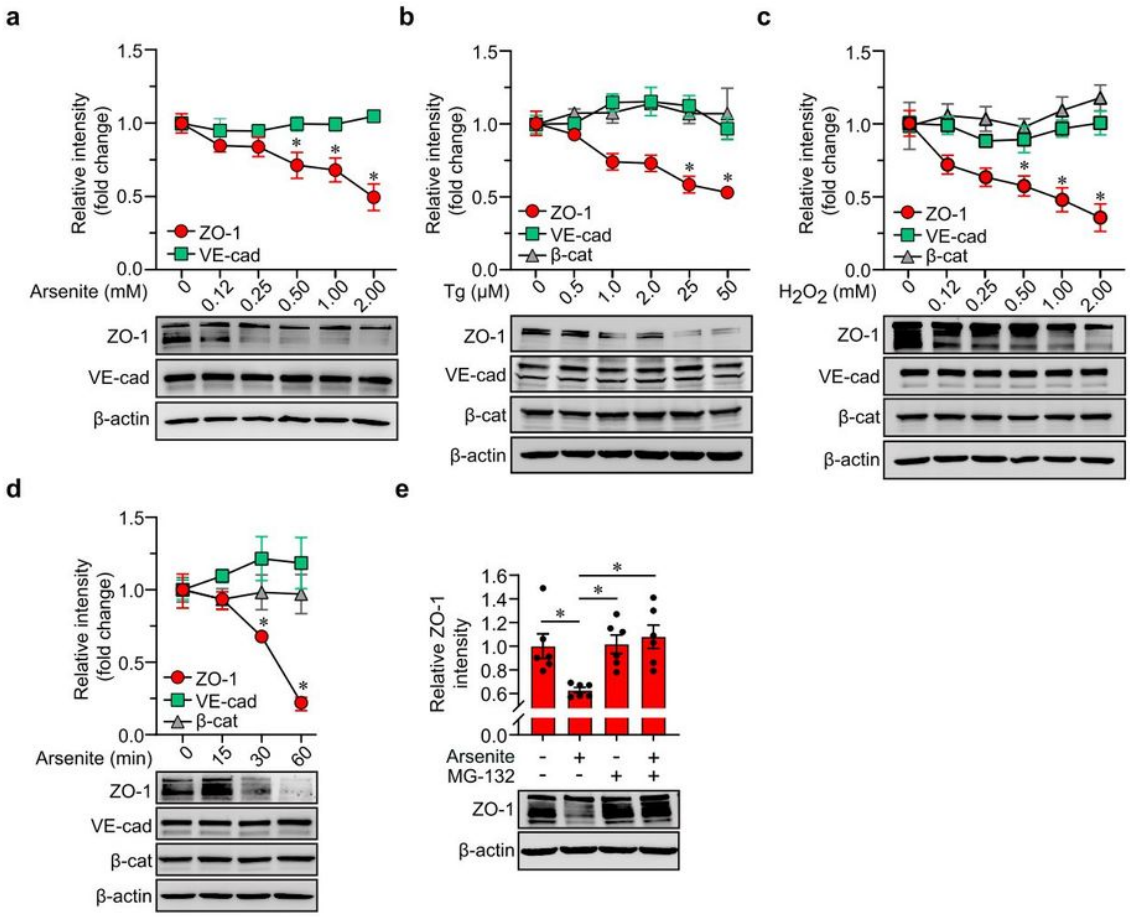

Figure 3

Stress-inducing treatments decrease ZO-1 expression levels in ECs.

a, b, c, Effects of increasing concentrations of arsenite (30 min) (**a**), thapsigargin (2 hr) (**b**) or H_2O_2 (30 min) (**c**) on expression levels of ZO-1, VE-cadherin and β-catenin in HUVECs (**a** and **c**) or BAECs (**b**). Protein expression levels were determined by western blot. β-actin serves as a loading control. **d**, Kinetics of the effects of arsenite treatment (500 μM) on expression levels of ZO-1, VE-cadherin and β-catenin in HUVECs. Protein expression levels were determined by western blot. β-actin serves as a loading control. **e**, Effect of the proteasome inhibitor MG132 (40 μM for 60 min) on arsenite-induced (500 μM for 30 min) downregulation of ZO-1 in HUVECs. ZO-1 expression levels were determined by western blot. β-actin serves as a loading control. **a-e,** Each point of the line graphs refers to the quantification of protein levels, represented as mean ± SEM relative to β-actin; * $p<0.05$. (**a**) n=5, (**b**) n=3, (**c**) n=4, (**d**) n=4 and (e) n=6 independent experiments.

Fig.4

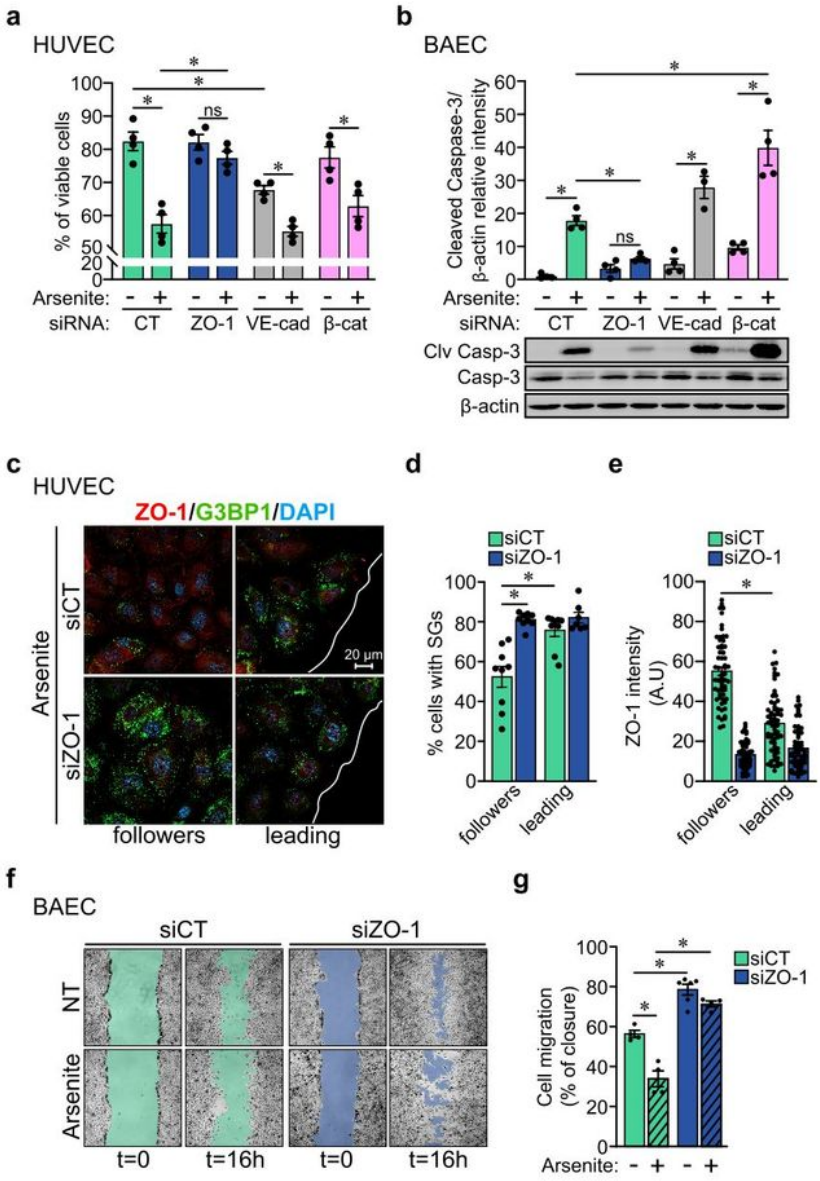

Figure 4

ZO-1 depletion increases viability and protects ECs against cellular stress.

a, Cell viability, measured by Trypan blue exclusion, of HUVECs transfected with siRNA against ZO-1, VE-cadherin or β-catenin and treated or not with arsenite (25 μM; 12 hrs). **b**, Immunoblot analysis of cleaved caspase-3 levels in siCT, siZO-1, siβ-catenin and siVE-cadherin transfected BAECs with siRNA and treated

or not with arsenite (50 μM; 6 hrs). Histogram referring to the quantification of cleaved caspase-3 levels relative to β-actin. Efficacy of siRNA-mediated knockdowns is shown in Supplemental Fig. S3a. **c,** Effects of arsenite treatment on migrating ECs. Immunofluorescence analysis of SGs formation and of ZO-1 levels in siCT or siZO-1 transfected HUVECs treated with arsenite (500 μM) and subjected to a wound healing migration assay for 30 min. Images of immunofluorescence staining of G3BP1 and ZO-1 of cells in 1^{st} and 2^{nd} rows (leading) and in 3^{rd} to 7^{th} rows (followers) relative to the edge of the wound (white line) are shown. Nuclei were stained with DAPI. **d,** The percentage of cells with SGs was calculated in leading and follower migrating cells as shown in (**c**). Results are from nine 40× fields per condition from 4 independent experiments. **e,** ZO-1 fluorescence intensity was measured in leading and follower migrating cells as shown in (**c**). Results are from at least fifty cells per condition in three independent experiments. **f,** Images of wound healing migration assays of BAECs transfected with siCT and siZO-1 treated or not with arsenite (10 μM). Images were taken immediately after wounding of the cell monolayer (t=0) and after 16 hours of migration (t=16h). **g,** Quantification of the percentage of wound closure at 16 hours of migration shown in (**f**). Histogram showing the average migration from 4 or 5 wound images per conditions. This experiment was repeated 3 times with identical results. **a, b, d, e, g,** Data are represented as mean ± SEM; * $p<0.05$.

Fig.5

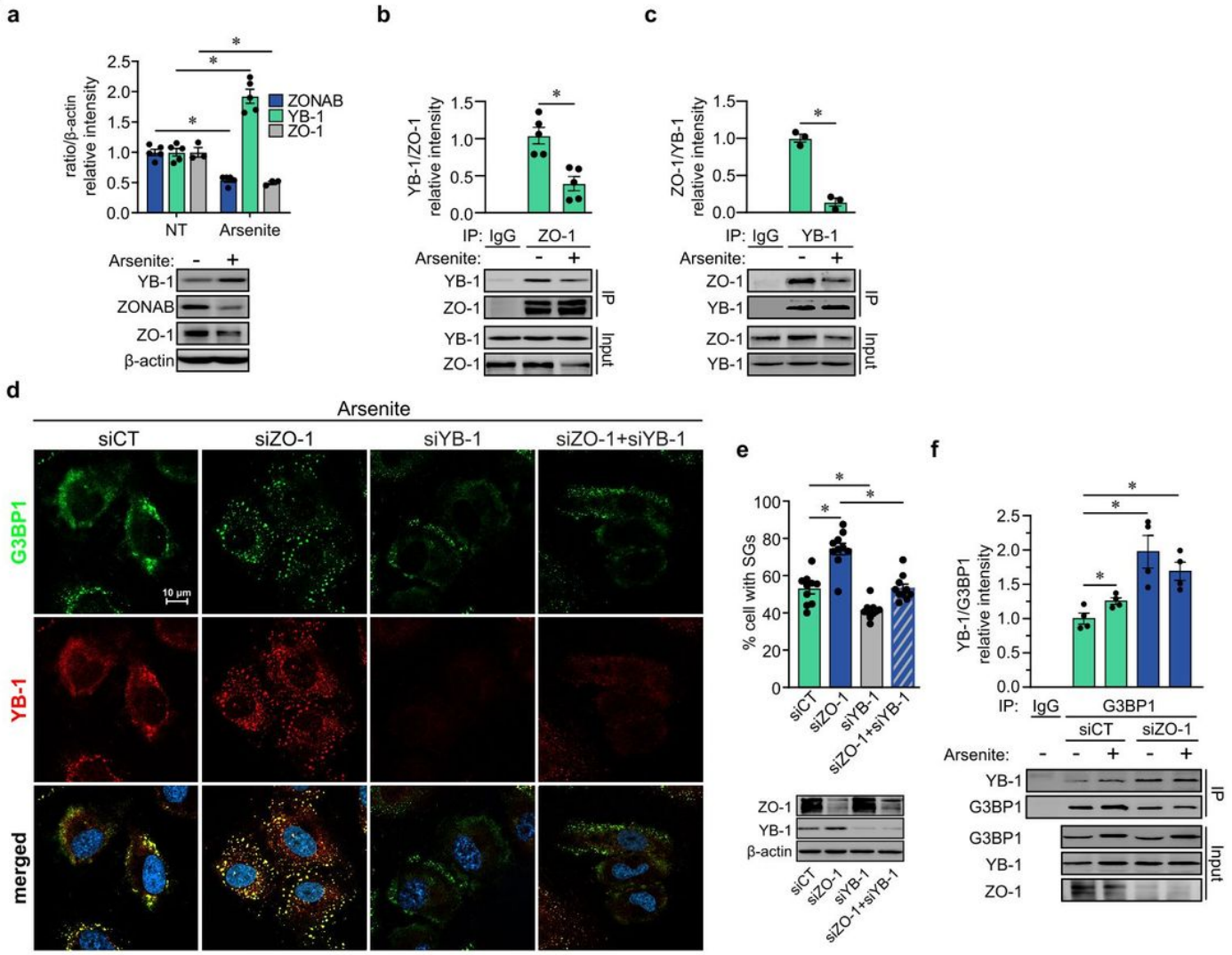

Figure 5

The ZO-1/YB-1 interaction regulates SG formation.

a, Effect of arsenite (50 μM; 6 hrs) on YB-1, ZONAB and ZO-1 protein levels in BAECs determined by immunoblot analysis. Histogram referring to the quantification of protein levels relative to β-actin. **b, c,** Effect of arsenite on YB-1 and ZO-1 association. ZO-1 (**b**) or YB-1 (**c**) were immunoprecipitated (IP) from lysates of BAECs treated or not with arsenite (500 μM; 30 min). Non-immune IgG serves as control for non-specific co-immunoprecipitation. Levels of immunoprecipitated proteins were determined by immunoblot using the indicated antibodies. Histograms show the quantification of the ratio of YB-1 levels relative to ZO-1 (**b**) or of ZO-1 levels relative to YB-1 (**c**) present in the immunoprecipitates. **d,** Decreased SG formation in YB-1 depleted cells. Images of immunofluorescence staining of SGs using antibodies against G3BP1 or against YB-1 in siCT, siZO-1, siYB-1 and combination of siZO-1 plus siYB-1 transfected HUVECs in presence of arsenite (500 μM; 30 min). Nuclei are stained with DAPI. **e,** Quantification of the SG formation shown in (**d**). The percentage of cells with SGs was calculated in 10 fields of 3 independent experiments. The downregulation efficiency of siRNA was confirmed by

immunoblot. **f,** Downregulation of ZO-1 increases the interaction between G3BP1 and YB-1. G3BP1 was immunoprecipitated (IP) from lysates of BAECs transfected with siCT or siZO-1 and treated or not with arsenite (500 μM; 30 min). Non-immune IgG serves as control for non-specific co-immunoprecipitation. Levels of immunoprecipitated proteins were determined by immunoblot using the indicated antibodies. Histogram showing the quantification of the ratio of YB-1 levels relative to immunoprecipitated G3BP1. Note that arsenite treatment increases G3BP1 levels in lysates. **a, b, c, e, f,** Data are represented as mean±SEM; * $p<0.05$.

Fig.6

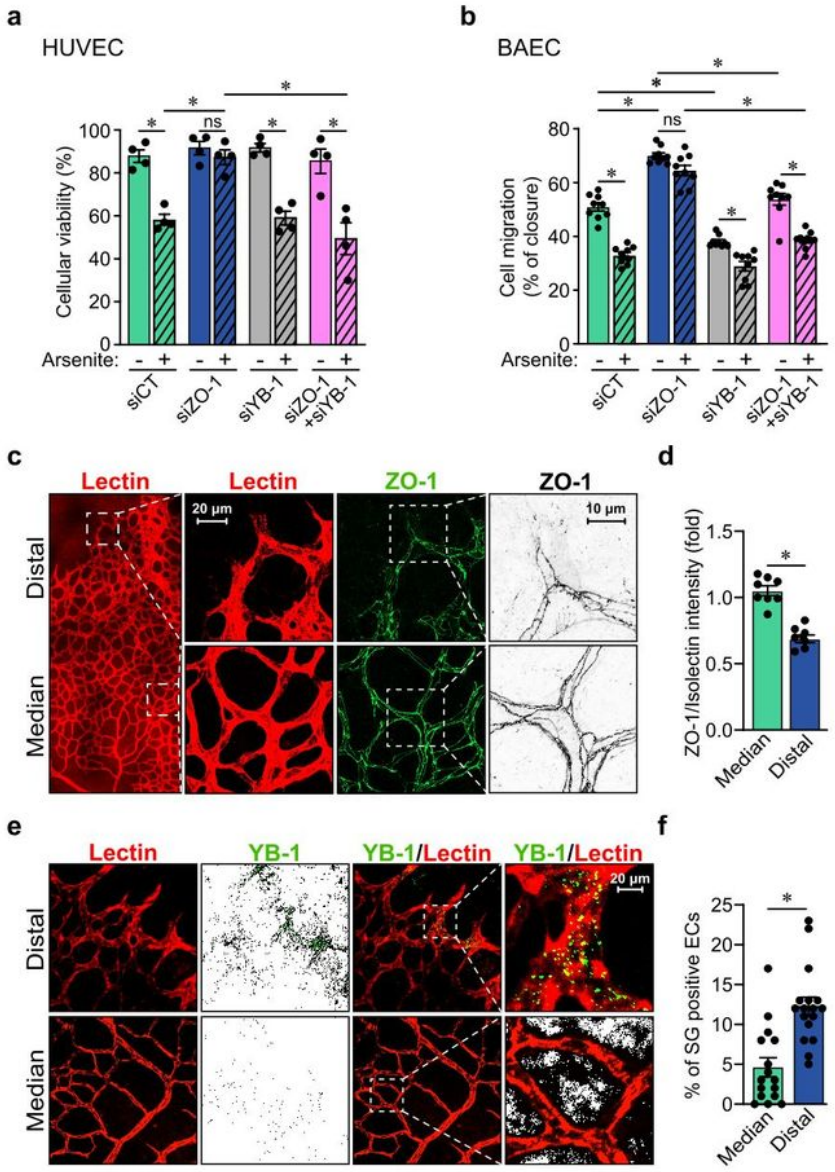

Figure 6

YB-1 is necessary for the cytoprotective effects of ZO-1 downregulation during retinal angiogenesis.

a, Cell viability, measured by Trypan blue exclusion, of HUVECs transfected with siRNA against CT, ZO-1, YB-1 or ZO-1 and YB-1 and treated or not with arsenite (25 µM; 12 hrs). **b,** Quantification of migration assays of BAECs transfected with siCT, siZO-1, siYB-1 or siZO-1 and YB-1 treated or not with arsenite (10

μM). Quantification of the percentage of wound closure at 16 hours of migration is shown. Histogram showing the average migration from 4 or 5 wound images per conditions. This experiment was repeated 3 times with identical results. **c,** Decreased ZO-1 levels in ECs of the distal portion of the developing retinal vasculature. Immunofluorescence analysis of ZO-1 levels in ECs of the distal (edge) and median (central) portions of the developing retinal vasculature (P7) of mice. Vascular ECs of the retinas were stained with Isolectin (red) and with antibodies against ZO-1 (green). For further clarity, right panels show the ZO-1 staining in black and white with intensities inverted. **d,** Quantification of images shown in (**c**). The results are presented as a ratio of the ZO-1/Isolectin intensity measured in 8 fields per portions of the retinas (median or distal) from 3 mice. **e**, Increased YB-1 positive SGs in ECs of the distal portion of the developing retinal vasculature. SGs were stained in ECs of the distal and median portion of the developing retinal vasculature (P7) of mice using antibodies against YB-1 (green). Vascular ECs of the retinas were stained with Isolectin (red). **f,** Quantification of SGs in retinal ECs shown in (**e**). Histogram showing the percentage of Isolectin-stained cells with SGs calculated from 16 fields of view of the distal and median portions of the retinal vasculature. This was done in retinas from 4 mice. **a, b, d, f,** Data are represented as mean±SEM; * $p<0.05$.

Supplementary Files

This is a list of supplementary files associated with this preprint. Click to download.

- TableS2.xlsx
- TableS1.xlsx
- SupplementalFiguresS1S5.pdf